
Article:
Akouibaa, M., Hassani, H.O., Ouarsal, R. et al. (6 more authors) (2022) (H3dien)[Ni(NO3)(C2O4)2].2H2O: Synthesis, crystal structure, catalytic activity and magnetic study. Chemical Data Collections, 42. 100969. ISSN: 2405-8300

https://doi.org/10.1016/j.cdc.2022.100969

(H3dien)[Ni(NO3)(C2O4)2].2H2O: Synthesis, crystal structure, catalytic activity and magnetic study

Mohamed Akouibaa[1], Hicham Oudghiri Hassani[1], Rachid Ouarsal[1], Souâd Rakib[1], Mohammed Lachkar[1], Morgane Poupon[2], Michal Dusek[2], Nicola Morley[3] and Brahim El Bali [4,*]

[1] Engineering Laboratory of Organometallic and Molecular Materials, Faculty of Sciences, University Sidi Mohamed Ben Abdellah, Po. Box 1796 (Atlas), 30000 Fez, Morocco.

[2] Institute of Physics of the Czech Academy of Sciences, Na Slovance 2, 182 21 Praha 8, Czech Republic.

[3] Department of Materials Science and Engineering, University of Sheffield, Sheffield S1 3JD, United Kingdom.

[4] Independent Scientist, Marrakech, Morocco; ORCID: 0000-0001-6926-6286,

Contact email: b_elbali@yahoo.com

Abstract

The complex $(H_3dien)[Ni(NO_3)(C_2O_4)_2].2H_2O$, with (dien) is a diethylenetriamine, and was synthesized in solution. It was characterized using single-crystal X-ray diffraction, Infrared (FT-IR) and UV-Visible spectroscopies, and TG-DTA thermal analysis. FT-IR confirmed the characteristic bands of diethylenetriamine, nitrate and oxalate groups. $(H_3dien)[Ni(NO_3)(C_2O_4)_2].2H_2O$ crystallizes into the monoclinic system ($P2_1/c$). Nickel has a square-based pyramidal NiO_5 coordination. O-H...O and N-H...O H-bonds connect molecules of the structure into slabs parallel to the bc-plane. The UV-Visible spectrum shows absorption bands compatible with a six-coordinated high-spin octahedral Ni(II). Magnetization and a.c. susceptibility measurements were measured. The catalytic efficiency of the title compound in the reduction by $NaBH_4$ of three nitrophenol isomers to their corresponding aminophenols was tested.

Keywords: Hybrid material; Crystal structure; Spectroscopy; Magnetism; Catalysis.

Graphical abstract

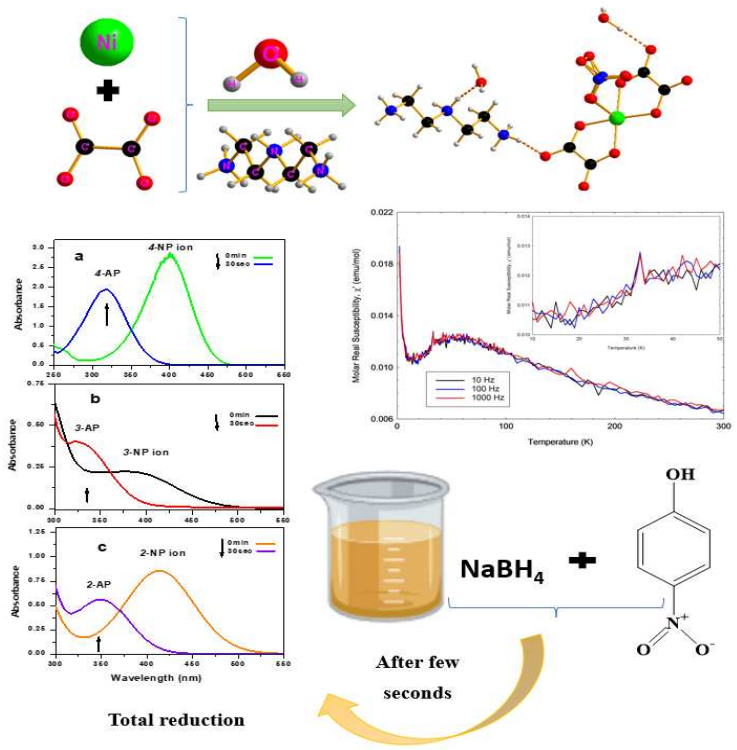

Keywords: Hybrid material; Crystal structure; FT-IR; TGA-DTA; Magnetism; Catalysis

Specifications Table	
Subject area	*Chemical Engineering.*
Compounds	$(H_3dien)[Ni(NO_3)(C_2O_4)_2].2H_2O$: diethylenetriammonium nitrato-bis(oxalato)nickelate(II)dihydrate
Data category	*Synthesis, crystallography, physico-chemistry studies.*
Data acquisition format	*Raw and simulated.*
Data type	*XRD, IR, UV-Visible, ATG-ATD, Magnetization and susceptibility, efficiency parameters.*
Procedure	*Wet chemistry synthesis, single and powder X-Rays characterizations, Infrared spectroscopy (FT-IR), UV-Visible spectroscopy and thermal stability analysis (TG-DTA), magnetic simulation, catalytic efficiency .*
Data accessibility	*Crystallographic data are deposited at CCDC.*

1. Rationale

During the last decades, the synthesis of hybrid materials has attracted considerable interest due to their new structural topologies, applications in the fields of catalysis, ion exchange and biochemistry [1-6], and interesting magnetic properties [7, 8]. Among these, a large number of open-framework compounds are based on metal phosphates [9], carboxylates [9-11], aliphatic and aromatic dicarboxylic acids [12, 13]. Over the past two decades, particular interest has been given to the extensive network structures formed by transition metal oxalates containing organic amines, with layered and other architectures [14-18]. Recently, the synthesis and crystal structures of oxalates of nickel (II), copper (II), tin (II) and zinc (II) were published [19-25].

In the present work, we report on the crystal structure of diethylenetriammonium nitrato-bis(oxalato)nickelate(II)dihydrate, $(C_4H_{15}N_3)[Ni(NO_3)(C_2O_4)_2].2H_2O$, referred to as $(H_3dien)[Ni(NO_3)(C_2O_4)_2].2H_2O$, with (dien = diethylenetriamine), referred below as complex (**1**). We discussed its thermal stability and spectroscopic features in correlation with its crystal structure. We also described the results of its application as a catalyst in reducing three nitrophenol isomers (ortho-, meta-, and para-) by $NaBH_4$ to their corresponding aminophenol isomers.

2. Procedure

*2.1 Synthesis of complex **1***

Single crystals of complex **1** were synthesized by a wet chemistry method. The reaction mixture of $Ni(NO_3)_2.6H_2O$ (0.34 g, 1.41 mmol) dissolved in distilled water (10 mL) was added dropwise to an aqueous solution (15 mL) of oxalic acid (0.52 g, 2.82 mmol) at room temperature with continuous stirring. Diethylenetriamine (1.7 mL, 15.60 mmol) dissolved in distilled water (15 mL) was dropwise added. This solution was then allowed to evaporate slowly until blue single-crystals were formed. These crystals were washed several times with cold water followed by ethanol and dried in the open air.

2.2. Characterizations

Complex **1** was characterized by single-crystal X-ray diffraction, Infrared spectroscopy (FT-IR), UV-Visible spectroscopy, thermal stability analysis (TG-DTA) and a.c. susceptibility.

2.2.1. Single crystal study

A suitable crystal, with the dimensions (mm): 0.19 × 0.16 × 0.12, was selected for X-ray diffraction analysis. Data were collected at room temperature with an Oxford diffraction CCD diffractometer Gemini using graphite-monochromated MoK_α radiation (λ = 0.7173 Å), registered with an Atlas S2 CCD area detector. The data were processed using the program Crysalis RED [26]. The phase problem was solved by direct methods using Superflip [27], and the structure was refined with Jana2006 [28]. Hydrogen atoms bonded to carbon were refined as riding atoms, using the constraint $U_{iso}(H) = 1.2\ U_{eq}$(parent atom). The same

constraint was applied to hydrogen atoms bonded to carbon and nitrogen, but their positions were refined freely. The nitrate anion was found disordered between two positions. The disorder was modeled by Jana2006 software using a rigid body NO_3 placed to two refinable positions, keeping the total occupancy equal to one [refined occupancies 0.723(13) and 0.277(13)]. The two free water molecules were fully occupied. The structural graphics were created using the DIAMOND program [29]. Crystal data collection and refinements details of complex **1** are summarized in Table 1. Atomic coordinates and basic geometrical data are reported respectively in Table 2 and Table 3, while the hydrogen bonds are given in Table 4. [Further details can be found in the deposited CIF at CCDC, with the code **CCDC 2031050**, using the link: www.ccdc.cam.ac.uk or from the Cambridge Crystallographic Data Centre, 12 Union Road Cambridge CB2 1EZ, UK; fax: +44 1223 336033; E-mail: deposit@ccdc.cam.ac.uk].

Table 1: Crystal data and crystal structure refinement parameters for complex **1**.

$C_8H_{20}N_4NiO_{13}$	F(000) = 912
M_r= 439 g.mol^{-1}	d_x= 1.783 g.cm^{-3}
Monoclinic, $P2_1/c$	Mo Kα radiation, λ = 0.71073 Å
a = 10.2176 (10) Å	Cell parameters from 3562 reflections
b = 11.0741 (11) Å	θ = 3.9-28.8°
c = 14.8967 (12) Å	μ= 1.27 mm^{-1}
β = 103.988 (8)°	T = 299 K
V = 1635.6 (3) Å^3	Z = 4
Data collection	
3896 independent reflections, 2840 with $I > 3\sigma(I)$	θ_{min} = 3.3 ° θ_{max}= 29.5 °
ωscans	R_{int}= 0.028
T_{min} = 0.957, T_{max} = 1	h= -12→14 k= -14→14 l = -20→19
11227 measured reflections	
Refinement	
Refinement on F_2	H atoms treated by a mixture of independent and constrained refinement
R[$F_2 > 3\sigma(F_2)$]= 0.033	Weighting scheme based on measured s.u.'s w= $1/(\sigma^2(I) + 0.0004I_2)$
wR(F_2)= 0.080	$(\Delta/\sigma)_{max}$= 0.043
S= 1.35	$\Delta\rho_{max}$ = 0.60 e Å^{-3}
3896 reflections	$\Delta\rho_{min}$= -0.64 e Å^{-3}
272 parameters	Extinction correction: B-C type 1 Gaussian isotropic (Becker & Coppens, 1974)
12 restraints	Extinction coefficient: 1000 (300)
86 constraints	

Table 2: Fractional atomic coordinates and their displacement parameters (Å2) for complex **1**.

	x	y	z	Uiso*/Ueq	Occ. (<1)
Ni1	0.36875 (3)	0.59106 (2)	0.027732 (19)	0.02257 (10)	
O1	0.38529 (18)	0.33214 (13)	0.20806 (11)	0.0321 (6)	
O2	0.33882 (17)	0.85766 (13)	−0.14732 (11)	0.0298 (6)	
O3	0.33122 (18)	0.24049 (13)	0.03198 (11)	0.0342 (6)	
O4	0.38082 (18)	0.94229 (14)	0.03017 (12)	0.0335 (6)	
O5	0.38670 (16)	0.51584 (13)	0.14795 (10)	0.0282 (6)	
O6	0.9429 (2)	0.59251 (19)	0.14787 (16)	0.0523 (8)	
O7	0.1774 (2)	0.73179 (17)	0.19306 (13)	0.0407 (7)	
O8	0.881 (2)	0.4051 (12)	0.0121 (12)	0.0468 (6)	0.35
O8'	0.8799 (11)	0.3972 (7)	0.0051 (6)	0.0468 (6)	0.65
O9	0.8940 (8)	0.2096 (10)	0.0090 (9)	0.0468 (6)	0.35
O9'	0.9198 (5)	0.2053 (5)	0.0075 (4)	0.0468 (6)	0.65
N1	0.0659 (2)	0.95922 (19)	0.20046 (15)	0.0286 (7)	
O10	0.39953 (17)	0.75174 (13)	0.08023 (11)	0.0299 (6)	
N2	−0.3040 (2)	0.88865 (18)	0.12833 (14)	0.0243 (7)	
O11	0.35128 (16)	0.67055 (13)	−0.09093 (10)	0.0277 (5)	
N3	0.4053 (2)	1.07803 (18)	0.19387 (15)	0.0256 (7)	
O12	0.35815 (17)	0.42663 (13)	−0.01948 (11)	0.0287 (5)	
N4	0.9372 (11)	0.3173 (7)	0.0441 (7)	0.0352 (9)	0.35
N4'	0.9295 (5)	0.2989 (3)	0.0483 (4)	0.0352 (9)	0.65
O13	1.0396 (6)	0.3247 (5)	0.1101 (4)	0.0468 (6)	0.35
O13'	0.9833 (3)	0.3020 (3)	0.1335 (2)	0.0468 (6)	0.65
C1	0.1650 (2)	1.0270 (2)	0.16200 (17)	0.0301 (8)	
C2	−0.0710 (2)	0.9524 (2)	0.13676 (18)	0.0309 (8)	
C3	0.2985 (2)	1.0264 (2)	0.23343 (17)	0.0321 (8)	
C4	−0.1648 (2)	0.8921 (2)	0.18693 (17)	0.0313 (8)	
C5	0.3753 (2)	0.40094 (19)	0.14247 (15)	0.0227 (7)	
C6	0.3539 (2)	0.78509 (19)	−0.08280 (16)	0.0220 (7)	
C7	0.3796 (2)	0.8328 (2)	0.01770 (16)	0.0237 (7)	
C8	0.3510 (2)	0.3499 (2)	0.04303 (15)	0.0241 (7)	
H1c1	0.134677	1.108695	0.149555	0.0361*	
H2c1	0.175476	0.987974	0.106616	0.0361*	
H1c2	−0.066821	0.90559	0.083277	0.0371*	

H2c2	−0.102818	1.032486	0.118841	0.0371*
H1c3	0.290615	1.07322	0.286114	0.0386*
H2c3	0.321753	0.944999	0.253115	0.0386*
H1c4	−0.134263	0.811326	0.203404	0.0376*
H2c4	−0.163689	0.935585	0.242876	0.0376*
H1n2	−0.362 (2)	0.865 (2)	0.1689 (17)	0.0292*
H2n2	−0.328 (2)	0.963 (2)	0.1066 (17)	0.0292*
H3n2	−0.311 (2)	0.836 (2)	0.0774 (17)	0.0292*
H1n3	0.488 (3)	1.071 (2)	0.2336 (18)	0.0307*
H2n3	0.408 (2)	1.041 (2)	0.1395 (18)	0.0307*
H3n3	0.395 (2)	1.158 (2)	0.1798 (17)	0.0307*
H1o6	0.931 (3)	0.542 (3)	0.104 (2)	0.0628*
H2o6	1.017 (3)	0.635 (3)	0.152 (2)	0.0628*
H1o7	0.210 (3)	0.729 (3)	0.149 (2)	0.0488*
H2o7	0.249 (3)	0.706 (2)	0.242 (2)	0.0488*
H1n1	0.055 (2)	1.002 (2)	0.2563 (18)	0.0343*
H2n1	0.095 (3)	0.884 (2)	0.2112 (17)	0.0343*

Table 3: Basic geometric parameters (Å, °) for complex **1**.

Ni1—O5	1.9432 (16)	N(1,2)—H2n(1,2)	0.89 (2)
Ni1—O10	1.9385 (15)	O11—C6	1.274 (3)
Ni1—O11	1.9438 (16)	N3—C3	1.475 (4)
Ni1—O12	1.9456 (15)	N3—H(1,3)n3	0.91 (2)
O1—C5	1.224 (3)	N3—H2n3	0.91 (3)
O2—C6	1.234 (3)	O12—C8	1.276 (3)
O3—C8	1.233 (3)	N4—O13	1.253 (11)
O4—C7	1.226 (3)	O10—C7	1.274 (3)
O5—C5	1.278 (3)	C6—C7	1.549 (3)
C1—C3	1.514 (3)	N1—C1	1.482 (3)
C2—C4	1.507 (4)	N1—C2	1.490 (3)
C5—C8	1.548 (3)	N2—C4	1.479 (3)
O8—N4	1.171 (17)	C—H	0.96

2.2.2. Infrared spectroscopy

IR spectra were recorded on a VERTEX-70 FT-IR spectrophotometer in the range 4000 to 400 cm^{-1} using the ATR technique with a resolution of 4 cm^{-1}.

2.2.3. UV-Visible spectroscopy

UV-Visible spectra were recorded using a Camspec M550 double beam scanning UV-Visible spectrophotometer in the range 280-850 nm.

2.2.4. TG-TDA analysis

Thermal stability analysis (TG-DTA) was carried out on a Diamond TDA-TGA instrument (Perkin-Elmer) thermal analyser (25-600°C) under air atmosphere at a scan rate of 10°C/min. Measurements were achieved on samples in an open platinum crucible under air flow.

2.2.5. Magnetization and a.c. susceptibility measurements

A MPMS-3 VSM-SQUID magnetometer was used to measure the magnetization and a.c. susceptibility of complex **1** as a function of magnetic field (up to 2 T) and temperature (between 2 to 300 K). The d.c. magnetization loops were measured at 5 and 300 K. The temperature dependence of the d.c. magnetization and a.c. susceptibility were measured between 2 and 300 K with an applied field of 100 Oe. Complex **1** was initially cooled down from 300 K to 2 K, in zero magnetic field, and a DC field of 100 Oe was then applied. For the zero-field cooled (ZFC) measurement, the magnetization and a.c. susceptibility were then measured as a function of temperature up to 300 K, between 2 K and 100 K, the data were measured every 1 K and above 100 K the data were measured every 5 K. The measurement was then repeated from 300 to 5 K for the field cooled (FC) data, with the same temperature steps. The ac susceptibility was measured using a 5-point measurement at 10, 100 and 1000 Hz at each temperature for both the ZFC and FC measurements.

2.3. Procedure for the reduction of nitrophenol isomers

The catalytic performance activity of complex 1 was tested in the reduction reaction of three nitrophenol isomers (4-nitrophenol, 3-nitrophenol, and 2-nitrophenol) to corresponding aminophenol isomers (4-aminophenol, 3-aminophenol, and 2-aminophenol) using sodium tetrahydroborate $NaBH_4$ at ambient temperature. In all three cases, the catalytic tests were conducted as follows: 40 mL of a nitrophenol isomer aqueous solution at 4×10^{-4} M was added under continuous stirring to 40 mL of a sodium tetrahydroborate $NaBH_4$ solution (8×10^{-4} M). An intense yellow color appeared due to the formation of the nitrophenolate ion, with an absorption peak located at 401, 393, and 415 nm for 4-NP, 3-NP, and 2-NP, respectively. The complex **1** (0.05 g) was then added to the aqueous solution under stirring, resulting in the disappearance of a dark yellow color solution. This reduction reaction was monitored with the help of a UV-Visible spectrophotometer.

3. Data, value and validation

3.1. Description of the structure

The crystal structure of $(H_3dien)[Ni(NO_3)(C_2O_4)_2].2H_2O$ is made up of $[Ni(C_2O_4)_2(NO_3)]^{3-}$ anions, diethylenetriammonium cations $(H_3dien)^{3+}$, and water molecules. The asymmetric unit contains 26 non-

hydrogen atoms (Figure 1), and it is isostructural with diethylenetriammonium bis(oxalato)cuprate(II) reported by Savel'eva *et al*. [30].

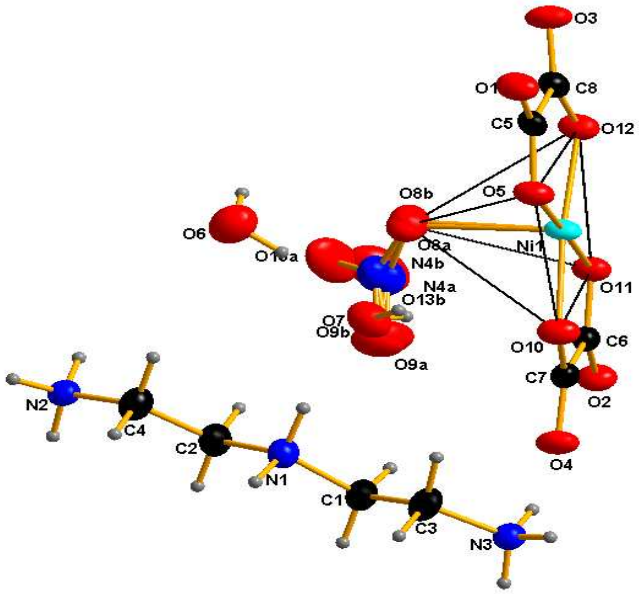

Figure 1: *The asymmetric unit of* $(H_3dien)[Ni(NO_3)(C_2O_4)_2].2H_2O$.

One nitrate and two oxalate ions are coordinating the Ni^{2+} respectively in monodentate, via the O8, and bidentate, through the couples (O5, O12) and (O10, O11) forming the square pyramidal unit $[Ni(C_2O_4)_2(NO_3)]$ (dsp_3 hybridization) as depicted in Figure 1. The closest none bonded oxygen atom, O12 from the neighboring $[Ni(C_2O_4)_2(NO_3)]$ unit at a distance 2.8286(16) Å changes the square pyramid into a distorted octahedron (d_2sp_3 hybridization) form, giving rise to a dimer (Figure 2). The square planar arrangement around the Ni^{2+} ion is slightly distorted, with O5-Ni-O11 and O10-Ni-12 angles 173.91(53) and 178.48(55)° (Table 3). On the other hand, according to the formula $\Delta_{oct}= 1/6\times\Sigma[(d_i-d_m)/d_m]_2$ [31, 32], the bond-length distortion for the octahedron is large, 2.6×10^{-3}, although still less than 6×10^{-3} found in $SrNi_2(PO_4)_2$ [33].

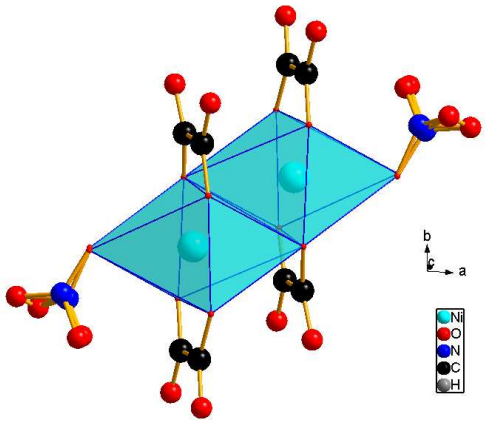

Figure 2: *A dimer in the crystal structure of* $(H_3dien)[Ni(NO_3)(C_2O_4)_2].2H_2O$.

The Ni^{2+} (d^8) rarely meets the square-pyramidal coordination where it acquires the hybridization sp^3d, and from the Cambridge Structural Database (CSD, update from November 2020) [34], a case where the square pyramidal coordination of Ni^{2+} is completed to (distorted) octahedron by another weak Ni-O interaction returns only one hit, FUSPAL [35], but the five Ni-O bonds forming the pyramid are below 2.1 Å while the bond referenced to be a weak interaction is about 2.4 Å. Thus, our structure is seemingly the only known example where the square NiO_5 pyramid with extremely long apical Ni-O bond length is completed to a form of an octahedron by weak Ni…O interaction.

However, CSD search for a bond or a weak interaction depends on the definitions given by the authors of the structure or the database internal mechanisms. More general searches can be done for NiO_4 fragments surrounded by another two oxygen atoms at a distance between 2.35 and 2.9 Å, without any assumptions about the character of the Ni…O interaction. Such searches returned 28 hits, some of them similar to our case, e.g. GIMHOA [36], RAMQUS [37], UWOJUN [38], and XILXIA [39]. NiO_4 planar fragment is completed into a form of octahedron by two long Ni-O bonds or weak interactions in all these cases. Among the structures found in the CSD, none has so different Ni-O distances like in the title structure. A question arises whether the Ni…O interaction with a very long Ni-O distance of 2.8286(16) Å contributes to the crystal packing. The bond valence sum for Ni [40] is 1.8327 Å with a square-pyramid coordination, and 1.9837 when the weak interaction is taken into account. Therefore, the Ni…O still contributes to the bond valence sum's exponential form despite its length. This indicates the interaction might play some role in the crystal packing.

O-H...O and N-H...O H-bonds connect molecules of the structure into slabs parallel to bc-plane (Figure 3 a&b and Table 4). If we do not consider the long Ni…O interaction, the connection of the slabs into a 3D network is made indirectly via the N2-H1N3…O5 hydrogen bonds. Figure 3c shows that the weak Ni…O interaction between two inversion-related $[Ni(C_2O_4)_2(NO_3)]$ units can contribute to this connection and justify the fact the structure is centrosymmetric. The water molecules participate in the packing of molecules in the slabs (Figure 3b). The water molecule with the oxygen O6 has hydrogen bonding with the

second water molecule O7, the disordered nitrate molecule and triprotonated $(H_3dien)^{3+}$ cation. The D…A distance is between 2.791 and 2.992 Å which correspond to a moderate hydrogen bond [41]. The second water molecule with the oxygen O7 has hydrogen bonding with the water molecule O6, the disordered nitrate molecule, the triprotonated $(H_3dien)^{3+}$ cation and two oxalate of $[Ni(C_2O_4)_2(NO_3)]$ units. The D…A distance is between 2.731 and 3.141 Å (Table 4) which correspond to a moderate hydrogen bond [41].

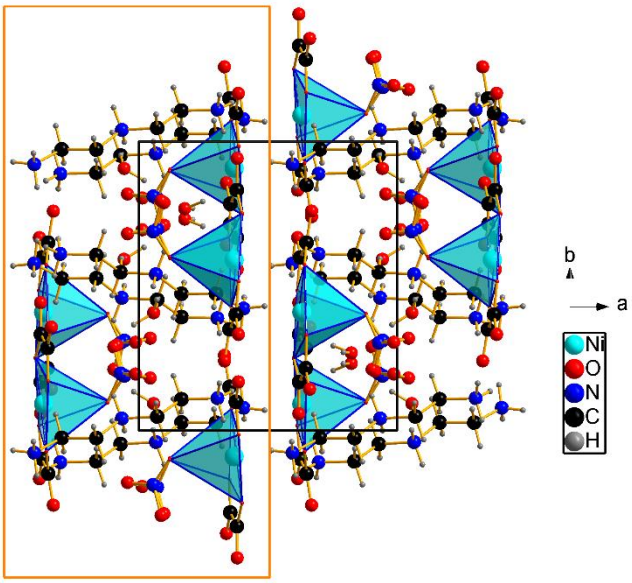

***Figure 3a**: Projection along b of the crystal structure of $(H_3dien)[Ni(NO_3)(C_2O_4)_2].2H_2O$.*

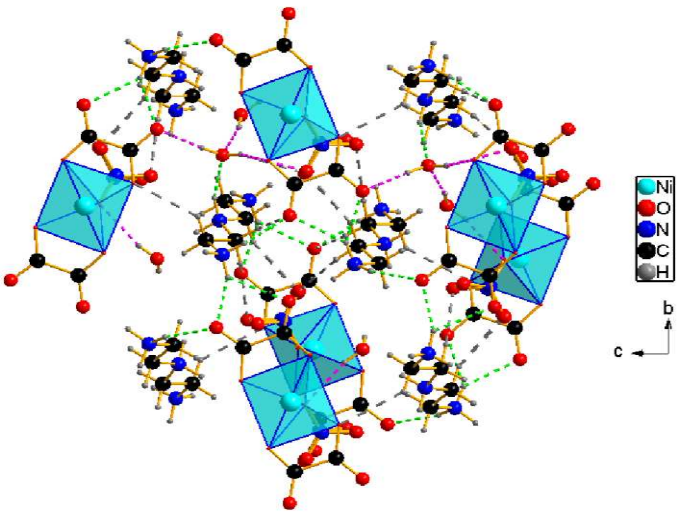

***Figure 3b**: A bc-parallel slab formed by molecules of the title structure connected by hydrogen bonds in the crystal structure of $(H_3dien)[Ni(NO_3)(C_2O_4)_2].2H_2O$. Dashed lines for H-Bonds: O-H...O (Pink), N-H…O (Green) and C-H…O (Grey).*

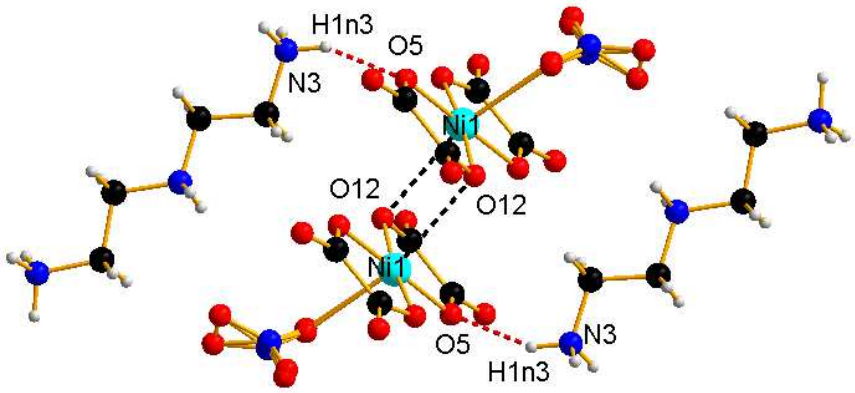

Figure 3c: *Weak interactions between two inversion-related [Ni(C₂O₄)₂(NO₃)] in the crystal structure of the title compound.*

Table 4: Hydrogen-bonds geometry (Å, º) within complex **1**.

D—H···A	D—H	H···A	D···A	D—H···A
N2—H1*n*2···O1$_{i}$	0.98 (3)	1.94 (3)	2.828 (3)	150.0 (19)
N2—H2*n*2···O2$_{ii}$	0.89 (2)	2.09 (2)	2.854 (3)	143 (2)
N2—H2*n*2···O4$_{ii}$	0.89 (2)	2.24 (2)	2.966 (3)	138 (2)
N2—H3*n*2···O3$_{iii}$	0.95 (2)	1.80 (3)	2.739 (3)	170 (2)
N3—H1*n*3···O5$_{iv}$	0.91 (2)	2.01 (2)	2.850 (2)	154 (3)
N3—H2*n*3···O4	0.91 (3)	1.92 (3)	2.824 (3)	168 (2)
N3—H3*n*3···O1$_{v}$	0.91 (2)	1.98 (2)	2.833 (3)	155 (2)
N3—H3*n*3···O3$_{v}$	0.91 (2)	2.33 (2)	2.957 (3)	126 (2)
N1—H1*n*1···O6$_{iv}$	0.99 (3)	1.74 (3)	2.718 (3)	171 (2)
N1—H2*n*1···O7	0.89 (2)	1.93 (2)	2.778 (3)	159 (3)
O6—H1*o*6···O8	0.85 (3)	2.02 (4)	2.860 (15)	169 (4)
O6—H1*o*6···O8′	0.85 (3)	2.15 (3)	2.992 (8)	170 (3)
O6—H2*o*6···O7$_{vi}$	0.88 (3)	1.93 (3)	2.791 (3)	165 (3)
O7—H1*o*7···O9$_{vii}$	0.80 (4)	2.44 (3)	2.992 (13)	127 (2)
O7—H1*o*7···O9′$_{vii}$	0.80 (4)	2.50 (3)	2.994 (7)	121 (2)
O7—H1*o*7···O10	0.80 (4)	2.42 (3)	3.141 (3)	151 (3)
O7—H2*o*7···O2$_{viii}$	0.94 (3)	1.82 (3)	2.731 (2)	161 (3)

Symmetry codes: (i) -*x*, *y*+1/2, -*z*+1/2; (ii) -*x*, -*y*+2, -*z*; (iii) -*x*, -*y*+1, -*z*; (iv) -*x*+1, *y*+1/2, -*z*+1/2; (v) *x*, *y*+1, *z*; (vi) *x*+1, *y*, *z*; (vii) -*x*+1, -*y*+1, -*z*; (viii) *x*, -*y*+3/2, *z*+1/2.

The bond lengths in the triprotonated $(H_3dien)^{3+}$ cation are in good agreement with the literature data on the known compounds containing similar cations [30]. The Ni-O(ox) (ox stands for oxalate) distances are in the range 1.9396(2)-1.9428(1) Å. These distances are similar to those found in a chain compound $(H_3dien)[Cu(NO_3)(C_2O_4)_2].2H_2O$ [30], Cu-O(ox) = 1.937(3)-1.942(3) Å. The distance Ni-O(n) (nitrate) for complex **1** of 2.4568(3) Å is comparable with its homolog in $(H_3dien)[Cu(NO_3)(C_2O_4)_2].2H_2O$, (2.467(4) Å) [30]. The distances recorded in the structure $(H_3dien)[Ni(NO_3)(C_2O_4)_2].2H_2O$ are within the usual range found in the complexes listed in the supplementary file (S1).

The distance C-O in the (ox)-ligands ranges from 1.225(7) to 1.276(2) Å, with shorter distances of non-coordinated oxygen atoms. The N-O distance in the NO_3 group is 1.230(2) and 1.261(2) Å, for the complex **1** the distance of C-O is approximately the same as in the copper oxalate compound 1.26(1) Å [30]. The average values of the C-C and C-N bond lengths are 1.51 Å and 1.48 Å, respectively, which conforms with the values reported in $(C_6H_{14}N_2)[Cu(C_2O_4)_2(H_2O)]\cdot 2H_2O$ [24]. The angles of CCN with terminal C atoms are larger than those in the middle of the chain by ~ 0.70 (110.1(2) and 110.8(2)°, as also found in the oxalate compound previously reported (111.2(4) and 108.7(4)° [30]).

3.2. Electronic spectrum

The electronic absorption spectrum of the $(H_3dien)[Ni(NO_3)(C_2O_4)_2].2H_2O$ complex, recorded in water (Figure 4) shows two bands in the visible region observed at 385 nm and around 700 nm corresponding respectively to the $^3A_{2g}(^3F) \rightarrow {}^3T_{1g}(^3P)$ and $^3A_{2g}(^3F) \rightarrow {}^3T_{1g}(^3F)$ spin allowed d-d transitions of the six-coordinated high-spin octahedral Ni(II), respectively [42]. The position of the two bands are in the same range reported for other related structures and are characteristic of octahedral geometry around Ni(II) ion [42,43]. The absorption band at the highest energy ($^3A_{2g} \rightarrow {}^3T_{1g}(^3P)$ have only a single maximum typical for octahedral complexes of nickel(II). However, the absorption band at the lowest energy ($^3A_{2g} \rightarrow {}^3T_{1g}(^3F), {}^1E_g$) shows an unusual band shape with two maxima 655 and 730 nm due to spin-orbit coupling that mixes the $^3T_{1g}(F)$ and ^1E_g states [44-47]. This assignment is in good agreement with the finding result obtained from X-ray structural determination of $(H_3dien)[Ni(NO_3)(C_2O_4)_2].2H_2O$ complex.

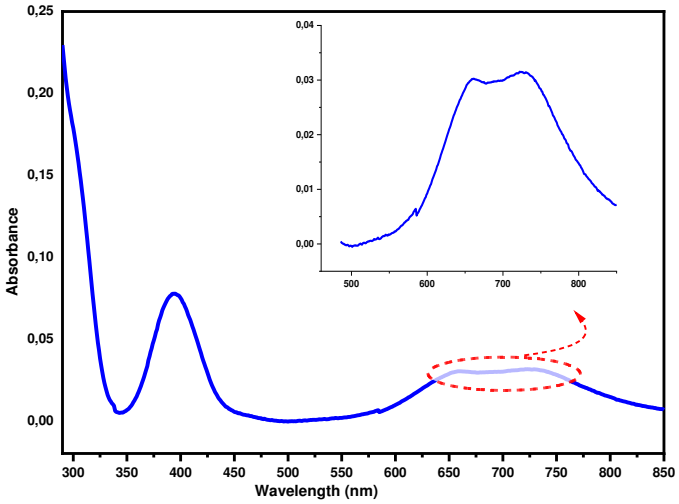

Figure 4. *UV-visible spectrum of $(H_3dien)[Ni(NO_3)(C_2O_4)_2].2H_2O$ complex in water at room temperature.*

3.3. Magnetic study

Low-dimensional systems are often studied due to being model objects for the verification of theoretical predictions in condensed matter physics theory and possible applications for tunable heat conduction for example [48]. This is because depending on where the transition metal ion sits within the structure, and the distance between these ions, a range of different exchange interactions can occur. If the ions have no interactions with each other, which will often occur above a Curie temperature, then paramagnetic behavior is observed. Below this Curie temperature, the ions can form short range and long range magnetic structures, depending on their exchange interaction. These magnetic structures include ferromagnetism where all the ions magnetic moments are aligned in the same direction, anti-ferromagnetism where the ions magnetic moments align anti-parallel to each other and ferrimagnetism where there are two sets of magnetic ions with different magnetic moments, that align anti-parallel to each other. To distinguish between the different magnetic orders, the magnetization as a function of magnetic field was taken at two temperatures (300 K, 5 K) and the d.c. magnetization and a.c. susceptibility were measured as a function of temperature, with a small applied magnetic field, for different applied frequencies, this allows for a complete analysis of the magnetic properties of materials [49].

Magnetization of $(H_3dien)[Ni(NO_3)(C_2O_4)_2].2H_2O$ as a function of the applied magnetic field was measured at the temperatures 5 and 300 K (Figure 5). For both temperatures, a linear behavior is observed, which means that the sample could either be paramagnetic or antiferromagnetic. According to the crystal structure study, the square $[NiO_5]$-pyramid being isolated in the framework, means that there are no direct interactions between the spin holders Ni^{+2} (d_8) (high spin: $t_{2g}^6e_g^2$) (Figure 5).

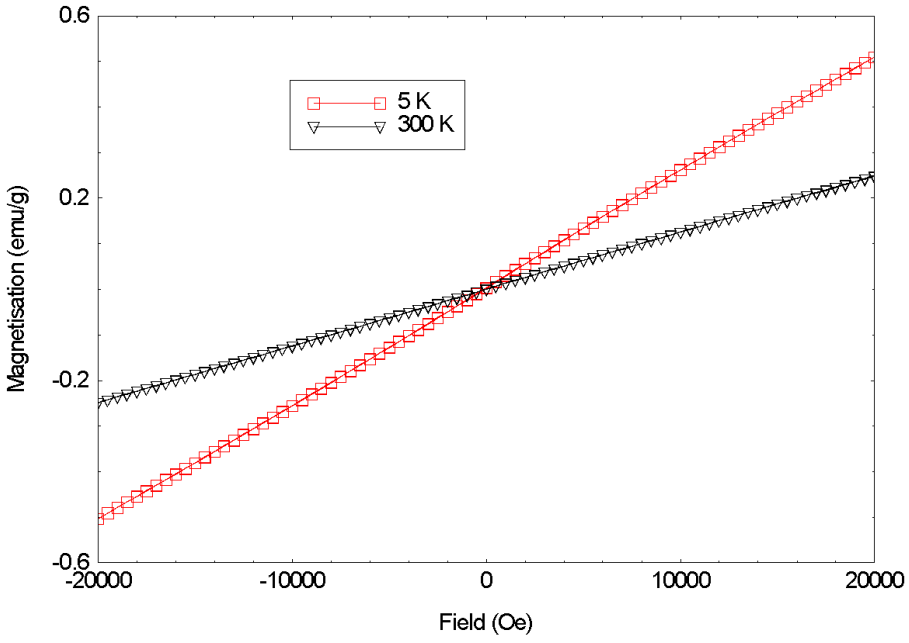

Figure 5: *Magnetization of $(H_3dien)[Ni(NO_3)(C_2O_4)_2].2H_2O$ as a function of magnetic field and temperature.*

Variable temperature a.c. and d.c. magnetization and a.c. susceptibility measurements of complex **1** were carried out on a powdered sample, from the grounded single crystals previously used for the structural determination and the other measurements, in the range 2 K-300 K (Figures 6 and 8). From room temperature, the real component of the molar susceptibility increases with decreasing temperature and reaches a first maximum at circa 50 K (Figure 8). This indicates a long magnetic order is established below this temperature. The results show also a transition at 32 K, with a minimum at 12 K, followed by a sharp rise in magnetisation and susceptibility. For the ZFC data, the transition at 32 K is only observed as a small peak in the magnetisation suggesting that the large increase in magnetisation at the same temperature in the FC data, requires the magnetic field to be applied for the alignment of the moments within the complex. For the ac magnetisation (measured at 10 Hz and 100 Oe), no transition is observed in the FC data, only a peak at 32 K, the same as the ZFC data (Figure 6 inset).

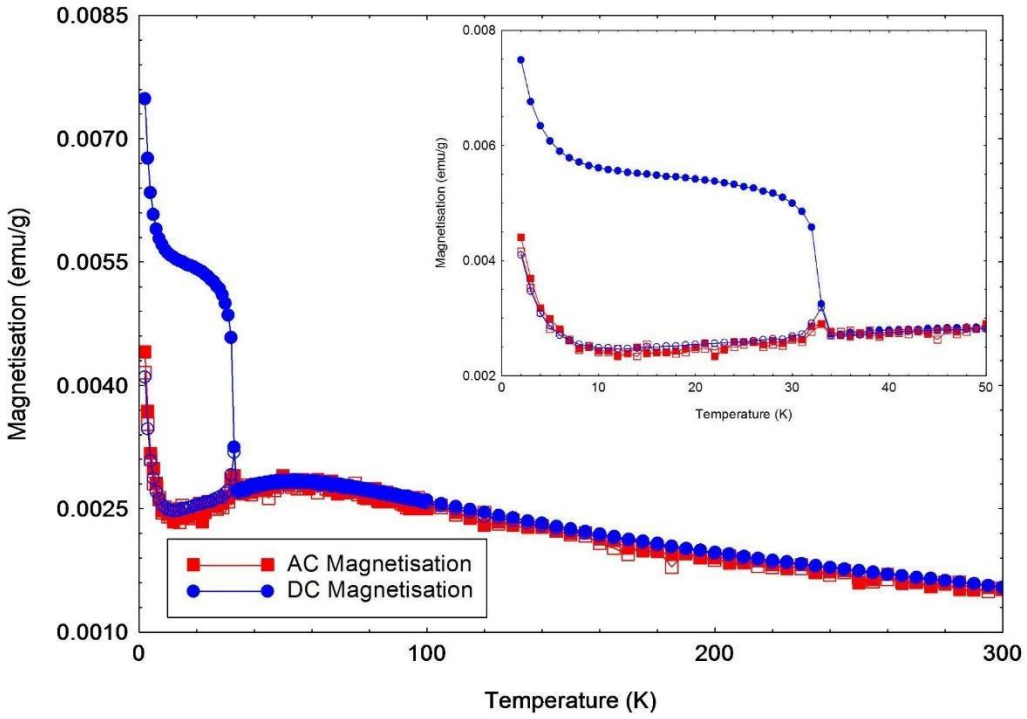

Figure 6: *Temperature-dependent magnetization of $(H_3dien)[Ni(NO_3)(C_2O_4)_2].2H_2O$ for an applied field of 100 Oe for both data sets. Inset: Magnetisation as a function of temperature for less than 50 K. The open shapes are for the zero field cooled (ZFC) data and the closed shapes are for the field cooled (FC) data. The AC magnetisation was measured for a frequency of 10 Hz*

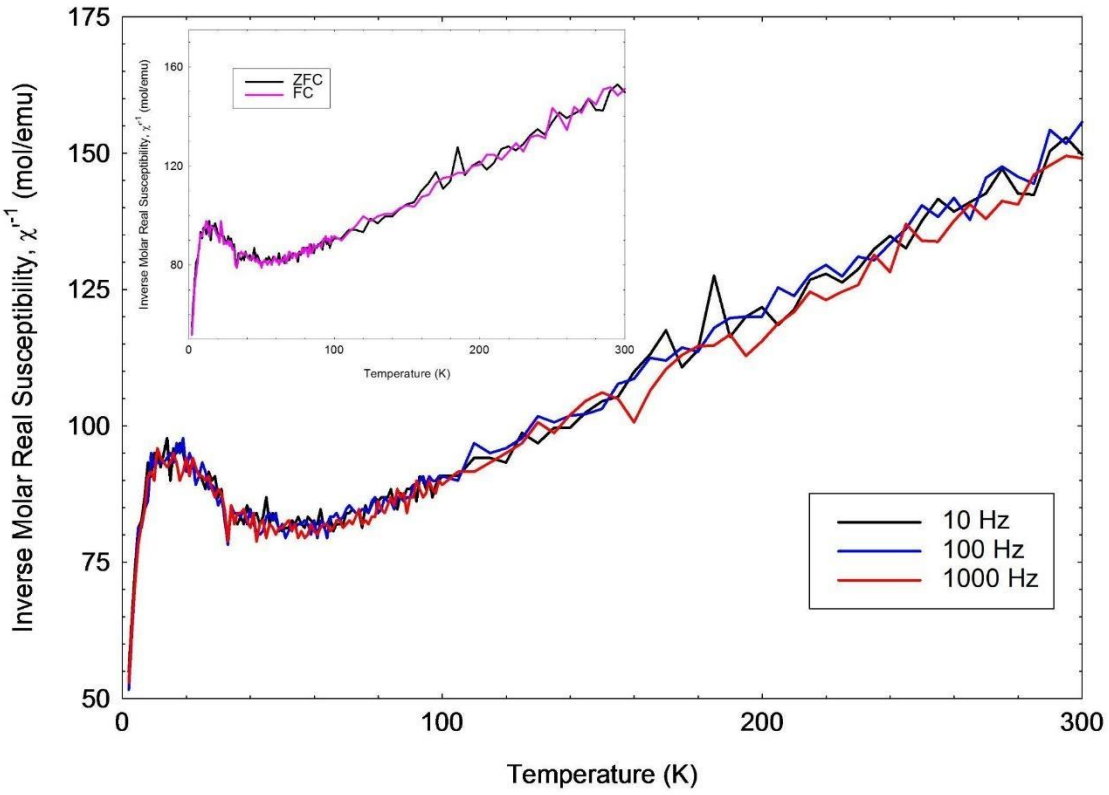

Figure 7: *Inverse molar real component susceptibility of $(H_3dien)[Ni(NO_3)(C_2O_4)_2].2H_2O$ versus temperature for an applied field of 100 Oe for three different AC frequencies, under ZFC conditions. Inset: Inverse molar real component susceptibility as a function of temperature for an applied field of 100 Oe and frequency of 10 Hz for ZFC and FC conditions.*

At high temperatures (T > 100 K), the thermal evolution of χ_m follows a Curie-Weiss law, given by the equation: $\chi = \chi_0 + C/(T-\theta)$, with χ_0 a temperature-independent component taking into account, inter alia, of the diamagnetism contribution of the compound, C the Curie constant and θ the Curie-Weiss temperature. The curve $\chi^{-1}(T)$ is mathematically fitted using the rearranged Curie-Weiss equation between 150 and 300 K. From this we get the magnetic constants (Curie-Weiss temperature θ_{CW}, Curie constant C and diamagnetic contributions χ_0) given in Table 5, the effective moment, μ_{eff} is determined, at 300 K, from the equation $\mu_{eff} = 2.828(\chi.T)^{1/2}$.

Table 5: *Magnetic constants of complex **1**.*

Magnetisation @20kOe, 300 K (emu/g)	Curie Constant	Weiss Constant (K)	Effective Moment (μB)
0.25	2.6	-132	3.56

For a free ion, the formula $\mu_{eff}(J) = gJ.[J(J+1)]_{1/2}$ is applied to determine the effective magnetic moment (μ_{eff}), with g the Landé gyromagnetic factor and J the total angular momentum (S + L). However, in the case of d-orbitals a splitting arises due to the crystal field, the effective moment is calculated either with the formula $\mu_S = 2\times[S(S+1)]_{1/2}$ when the orbital moment L is quenched (S is the spin-only effective moment), or using $\mu_{(S+L)} = [4S(S+1) + L(L+1)]_{1/2}$, in the case L is decoupled from S. The effective experimental μ_{eff} value of 3.56 μ_B per Ni^{2+} ion is larger compared to the spin-only value μ_{so} = 2.86 μ_B, most likely due to the strong spin-orbit coupling (L·S) often observed for high-spin Ni^{2+} and a strong magnetic anisotropy related to the triplet ground state [50-52]. The Curie-Weiss temperature value $\theta = -132$ K reveals an antiferromagnetic coupling between the spin holders. The sharp second peak at 32 K could be related to weaker inter-chains interactions, or spin glass behaviour but further investigations are required. If the material became a spin-glass at either of the peaks, it would be expected that the peak would shift in temperature as a function of frequency. For the peak at ~50 K, no change in peak position is observed with frequency, but there are two things to note, the first is that is a broad peak with width over ~20 K, which is unusual for a spin glass, as they would normally have a sharper peak with a width of a few Kelvins. Plus, the signal to noise ratio on the data is ~70, which means that any small shift is likely to have been masked by the noise. For the peak at 32 K (Figure 8 inset), no shift is observed in temperature with frequency, nor is there a change in the real component susceptibility magnitude, as would be expected for a spin glass. Further the ZFC and FC data for the ac real component have the same temperature dependence (Figure 7 inset), where it would be expected for a spin glass that the FC susceptibility dependence to differ to the ZFC dependence as observed in the dc magnetisation data.

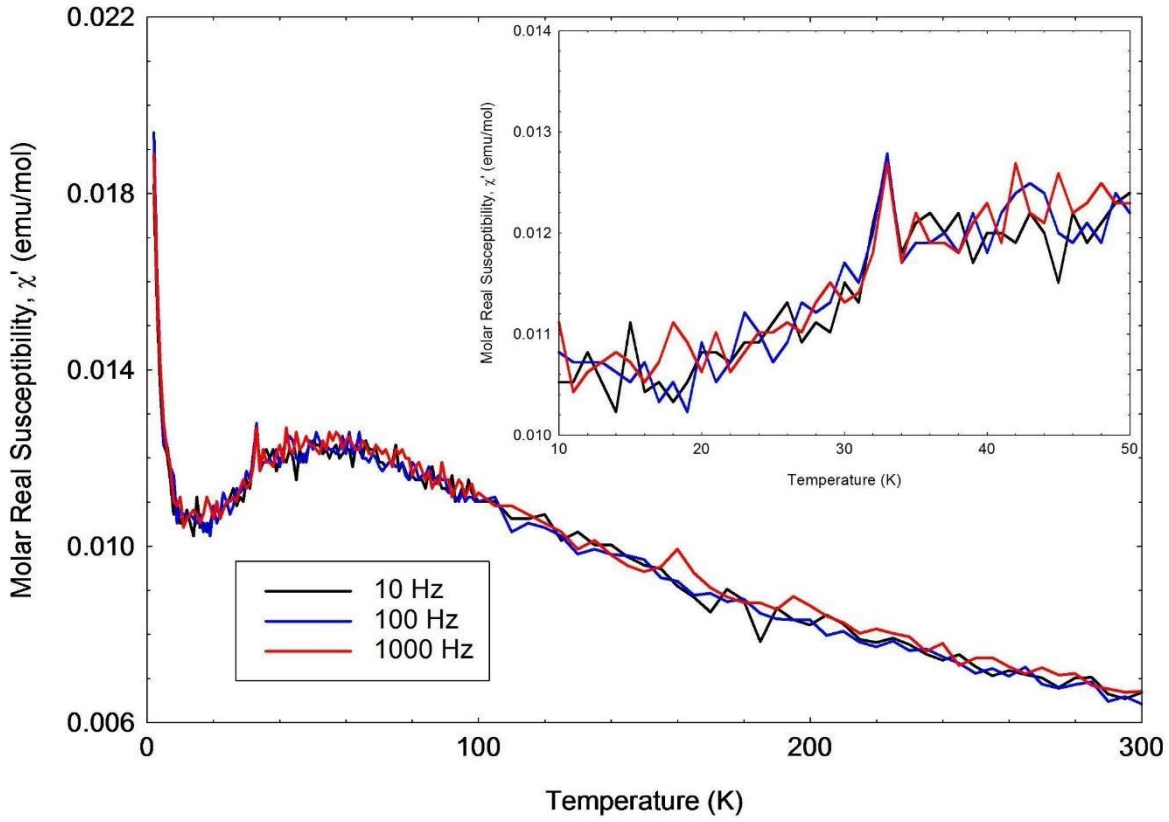

Figure 8: *Molar Real susceptibility of $(H_3dien)[Ni(NO_3)(C_2O_4)_2].2H_2O$ against temperature for an applied field of 100 Oe and for three different ac frequencies, under ZFC conditions. Inset: Molar real susceptibility as a function of temperature between 10 K and 50 K.*

3.4. Infrared spectroscopy

Infrared spectroscopy was used to distinguish various modes of coordination of the nitrate group and the presence of organic amine cations. Table 6 lists the infrared assigned bands for complex **1**. The IR spectrum of complex **1**, exhibits vibrational modes of the different entities, corresponding to the vibration of the diethylenetriamine, nitrate, water, and the oxalate groups (Figure 9). The FT-IR spectrum reveals the presence of two large bands ranging between 3302-2662 cm^{-1} and 1750-1035 cm^{-1}. The deconvolution method provides a detailed interpretation in terms of bands. Indeed, in accordance with the structure obtained by single crystal X-ray structure, the FT-IR spectrum shows the presence of all the functional groups present in the complex **1**. The vibrational modes at 3600 and 3485 cm^{-1} are assigned to the asymmetric and symmetric vibrations of the water molecule, while the band at 1620 cm^{-1} corresponds to $\delta(H_2O)$ [53]. The spectrum also reveals several bands corresponding to the oxalate group. The bands at 1712 and 1663 cm^{-1} are characteristic to the vibration of the asymmetric elongation ν_{as}(O-C-O) in the CO2 group. The band at 1341 cm^{-1} corresponds to the stretching vibration of the symmetric connection ν_s(O-C-O), while the one observed at 781 cm^{-1} corresponds to the vibration of the deformation δ_{as}(O-C-O) [54,

55]. The bands located at 3200 and 3126 cm^{-1} are attributed to the vibration of asymmetric and symmetric elongation of $\nu_{as}(-NH_2)$ and $\nu_s(-NH_2)$ linkage. The bands observed at 2813 and 2943 cm^{-1} correspond to the vibration of symmetric elongation of $\nu_s(-CH_2)$ [56], while the band observed at 3043 cm^{-1} is attributed to the vibration of elongation of ν_{as}(N-H) group of the protonated amine NH_{3+}. The band at 1138 cm^{-1} is attributed to the vibration of the deformation δNH_{3+}). In addition, those observed at 1582 and 1394 cm^{-1} correspond to the vibration of the deformation $\delta_{as}(-NH_2)$ and $\delta_{as}(-CH_2)$ [57]. The weak bands at 895, 663 and 1117 cm^{-1} are attributed respectively to the elongation vibrations ν(-NH) and ν(-CN) [58]. For the nitrate group, three vibration bands are observed. The bands located at 1510 and 1262 cm^{-1} correspond to the vibration of asymmetric and symmetric elongation $\nu_{as}(NO_2)$ and $\nu_s(NO_2)$, while the N-O stretching frequency is found at 996 cm^{-1}. Variable coordination modes of the nitrate ligand were observed in several series of complexes: the monodentate and bidentate chelate mode, which can be symmetrical or asymmetrical, and the bridged bidentate ligand [59-62]. The symmetry of nitrate anions differs slightly between C_{2v} and C_s. When the nitrate ion acts as a monodentate coordinating agent (C_{2v} symmetry) all bands become active, according to the literature [63, 64]. This confirms that the nitrate group was monodentate in complex **1**. Finally, the bands observed at 548 and 490 cm^{-1} correspond to the vibration of elongation (Ni-O), which is similar to those found in the literature [65, 66].

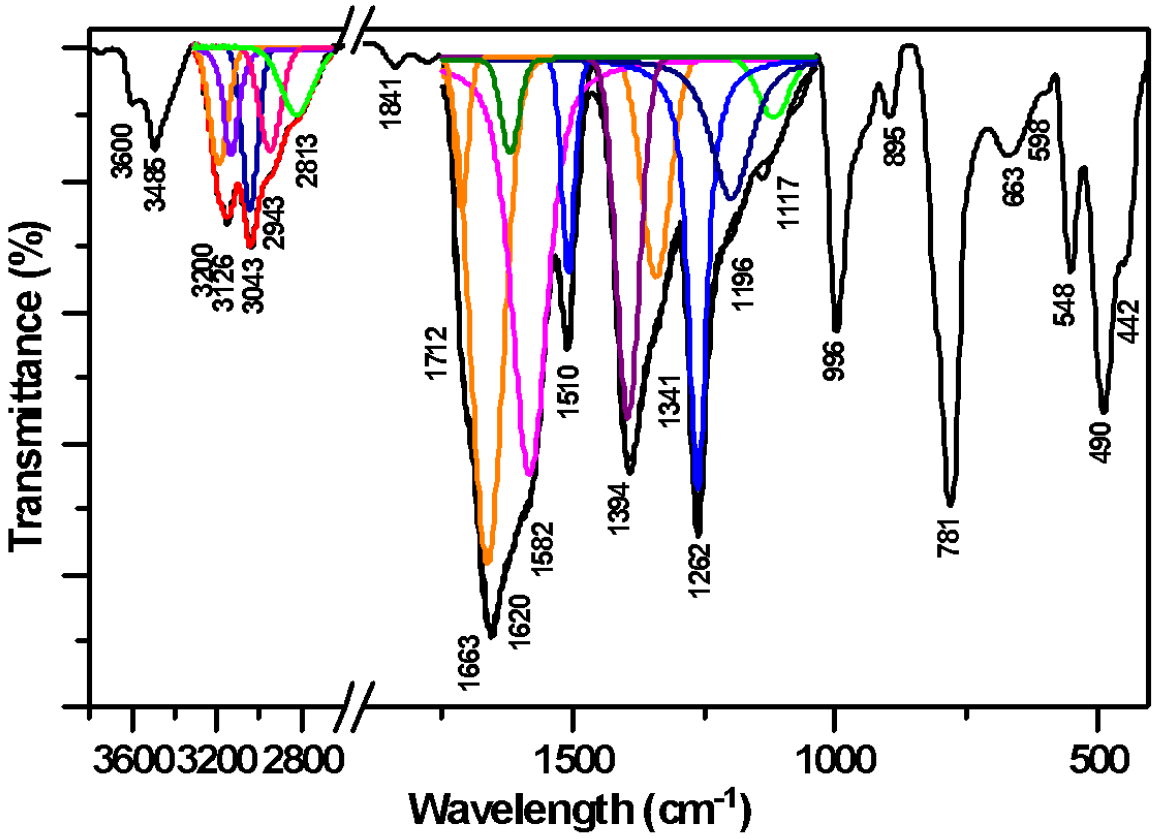

Figure 9: *Infrared spectrum of* $(H_3dien)[Ni(NO_3)(C_2O_4)_2].2H_2O$.

Table 6: *Bands assignments of the infrared spectrum of complex* ***1****.*

Bands (cm^{-1})	**Assignment**
1712 and 1663	ν_{as}(O-C-O)
1620	δ(H_2O)
1341	ν_s(O-C-O)
781	δ_{as}(O-C-O)
1510	ν_{as}(NO_2)
1262	ν_s(NO_2)
996	coordinated nitrate group (NO)
3200	ν_{as}(-NH_2)
3126	ν_s (-NH_2)
2813 and 2943	ν_s(-CH_2)
3043	ν_{as}(NH_{3+})
1138	δ?NH_{3+})
1582	δ_{as}(-NH_2)
1394	δ_{as}(-CH_2)
895 and 663	ν(-NH)
1117	ν(-CN)
1196	ν(-C-C)
3600	ν_{as}(H_2O)
3485	ν_s(H_2O)
548 and 490	ν(Ni-O)

3.5. Thermal analysis

Figure 10 depicts the TGA-DTA curve of complex **1**, which presents several weight losses. The first weight loss is related to the departure of two water, in accordance with calculated weight loss (observed 8.8%, calculated 8.2%). This step shows an endothermic process located at molecules 135°C, which refers to the weak hydrogen bond that holds water in the crystal structure, as already stated they are important in the crystal structure study. A second weight loss, observed with an endothermic process, occurs in the range of 140-225°C, which can be explained by deprotonation and volatilization of organic amine (dien) and nitrate groups (observed 38.40%, calculated 38.72%). The weight loss during further heating is carried out in two successive steps: the first is observed in the temperature range of 225-320°C and the second in 400-550°C, both with an exothermic process. The last weight loss can be attributed to the decomposition of oxalate to three carbon dioxide molecules 3CO_2(g), and the carbon monoxide molecule CO(g) (observed

36.6%, calculated 36.4%). The final decomposed product corresponds to the NiO (observed 16.2%, calculated 17%). The weight losses that refer to the decomposition of organic amine, nitrate group and a part of oxalate molecule of our studied compound were calculated using these equations below:

$$(C_4H_{16}N_3)[Ni(NO_3)(C_2O_4)_2].2H_2O \rightarrow (C_4H_{16}N_3)[Ni(NO_3)(C_2O_4)_2] + 2H_2O$$

$$(C_4H_{16}N_3)[Ni(NO_3)(C_2O_4)_2] \rightarrow (C_2O_4)Ni(C_2O_4) + C_4H_{16}N_3 + NO_3$$

$$(C_2O_4)Ni(C_2O_4) \rightarrow Ni(C_2O_4) + 2CO_2$$

$$Ni(C_2O_4) \rightarrow NiO + CO_2 + CO$$

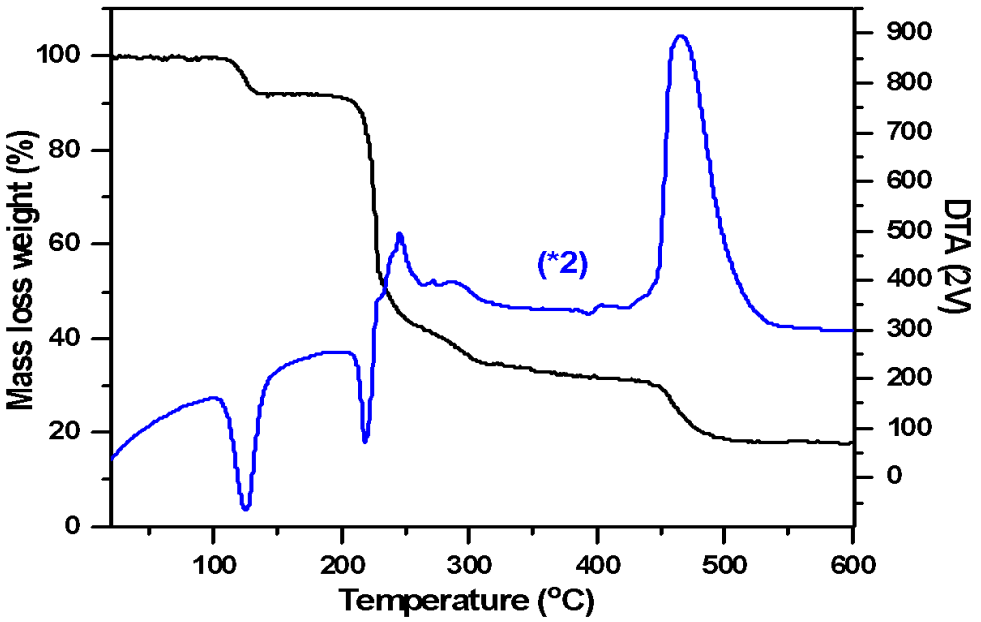

Figure 10: *TGA-DTA analyses of $(H_3dien)[Ni(NO_3)(C_2O_4)_2].2H_2O$.*

3.6. Nitrophenol isomers reduction test

Powder particles of complex **1** (**1**Ps) obtained from the grounded single crystals previously used for the structural determination are tested as a catalyst performance for the reduction reaction of three nitrophenol isomers (4-nitrophenol, 3-nitrophenol and 2-nitrophenol) with sodium tetrahydroborate $NaBH_4$. The results are presented in Figures 11 (a-c). Complex **1** was very efficient as a catalyst. In fact, at the beginning stage, when we mixed the nitrophenol isomers with sodium tetrahydroborate, phenolate anions were produced, which caused a strong coloration of the solution. No reduction was detected with the activity of sodium tetrahydroborate alone for several days. However, after the addition of the powder particles of complex **1**, the solution became uncolored in a few seconds for all of the three-nitrophenol isomers. The highest bands of absorption located at 401, 393, and 415 nm and corresponding respectively to 4-nitrophenol, 3-nitrophenol and 2-nitrophenol disappear in favor of new bands located at 317, 328, and 347 nm for the 4-aminophenol, 3-aminophenol and 2-aminophenol, respectively. In fact, at room temperature 30 seconds were necessary to achieve the reaction with the appearance of the corresponding

three aminophenol isomers. The obtained result exhibits the high catalytic performance of the synthesized diethylenetriammonium nitrato-bis(oxalato)nickelate(II)dihydrate in the reduction reaction of the nitrophenol isomers related to anterior research study discovered in the literature as mentioned in Table 7.

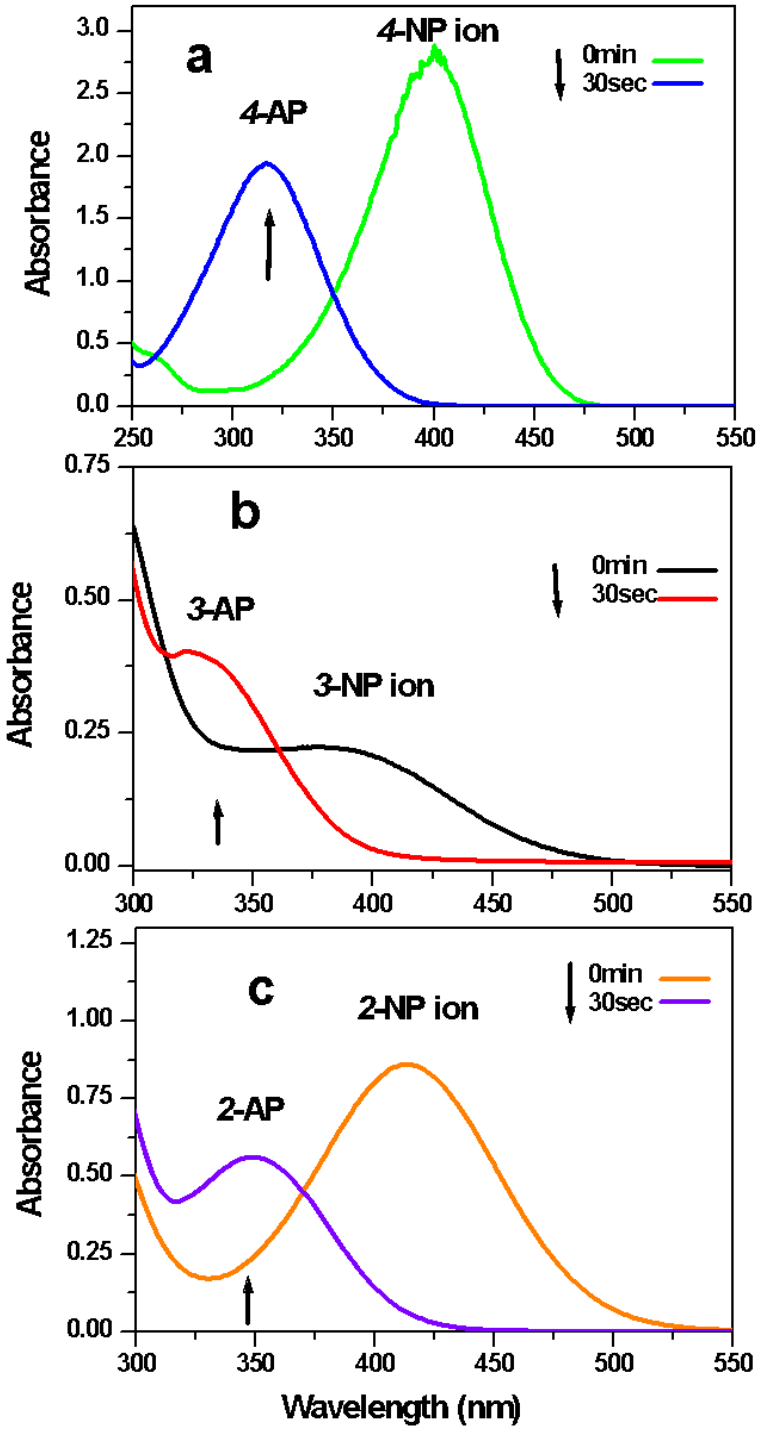

Figure 11: *UV-visible spectra of: (a) 4-nitrophenol (4-NP); (b) 3-nitrophenol (3-NP); and (c) 2-nitrophenol (2-NP) isomers in the presence of sodium tetrahydroborate $NaBH_4$ and after adding complex **1** at room temperature.*

Table 7: *Reduction of 4-NP 3-NP and 2-Np by complex **1**, a comparison of reaction time with known compounds.*

Catalyst	Type	Concentration of NP (mol/L)	Reaction Time (sec)	Reference
$(C_4H_{15}N_3)[Ni(NO_3)(C_2O_4)_2].2H_2O$	**Hybrid material**	**4×10^{-4}**	**30 for 4-NP** 30 for 3-NP 30 for 2-NP	**This work**
$(C_4H_{12}N_2)[Co(H_2O)_6](HPO_4)_2$	**Hybrid material**	**4×10^{-4}**	**240for 4-NP** 30 for 3-NP 240 for 2-NP	**[67]**
$NiMoO_4$	**Nanoparticles**	**2×10^{-4}**	**480 for 4-NP** 180 for 3-NP 480 for 2-NP	**[68]**
$NiFe_2O_4$	**Nanoparticles**	**3.6×10^{-5}**	**2280 for 4-NP** 2160 for 3-NP 1680 for 2-NP	**[69]**
Ni/C black	**Nanocomposites**	**5.0×10^{-4}**	**900 for 4-NP** **900 for 3-NP** **900 for 2-NP**	**[70]**
$ZnMoO_4$	**Nanoparticles**	**2×10^{-4}**	**60 for 3-NP**	**[71]**
$CuMoO_4$	**Nanoparticles**	**4×10^{-4}**	**840 for 4-NP** 360 for 3-NP 840 for 2-NP	**[72]**

A proposed mechanism for the studied reduction reaction can be assumed as follows: the BH_4^- is dissociated to form (**1**Ps)-H and (**1**Ps)-BH_3^- in the presence of the powder particles of complex **1** (**1**Ps) catalyst as reactive intermediates (Eq. 1) [73]. Accordingly, these intermediates (Eqs. 2 to 3) were responsible for the reduction of the nitrophenol isomers. In fact, 6 electrons are engaged in the transformation of the nitrophenol isomers (NP) to the related aminophenol (AP) for this reduction reaction.

$$2(\mathbf{1}Ps) + BH_4^- \rightleftharpoons (\mathbf{1}Ps)\text{-}H + (\mathbf{1}Ps)\text{-}BH_3^- \quad (1)$$

$$6(\mathbf{1}Ps)\text{-}H + NP \blacktriangledown AP + 6(\mathbf{1}Ps) + 6H^+ \quad (2)$$

$$6(\mathbf{1}Ps)\text{-}BH_3^- + NP \blacktriangledown AP + 6(\mathbf{1}Ps) + 6BH_3 \quad (3)$$

Previous similar research studies found in the literature, proposed the same mechanism for the reduction reaction of three nitrophenol isomers with sodium tetrahydroborate $NaBH_4$ using several catalysts [68,71-73].

4. Conclusion

A new open-framework diethylenetriammonium nitrato-bis(oxalato)nickelate(II) dihydrate $(H_3dien)[Ni(NO_3)(C_2O_4)_2].2H_2O$ was successfully synthesized using a soft chemistry route. The title compound was characterized by single-crystal X-ray diffraction, Infrared spectroscopy (FT-IR) and thermal stability analysis (TG-DTA). FT-IR confirmed the presence of the characteristic bands of diethylenetriamine, nitrate and oxalate groups. $(H_3dien)[Ni(NO_3)(C_2O_4)_2].2H_2O$ crystallizes in the monoclinic system, space group P21/c and its structure is described as a 3D framework in which dimers $[Ni(NO_3)(C_2O_4)_2]$ interact through the H-Bonds. The thermogravimetric analysis showed that the title complex is stable until 135°C. The magnetization and a.c. susceptibility of the sample as a function of magnetic field and temperature were measured and discussed. The new hybrid phosphate was found to be an effective catalyst for the reduction reaction of the three nitrophenol isomers.

Acknowledgement

The crystallographic part was supported by the project 18-10504S of the Czech Science Foundation using instruments of the CzechNanoLab Research Infrastructure supported by MEYS CR (LM2018110).

References

[1] P.J. Hagrman, D. Hagrman, J. Zubieta, Organic-Inorganic Hybrid Materials: From “Simple” Coordination Polymers to Organodiamine-Templated Molybdenum Oxides, Angew. Chem. Int. Ed. 38 (1999) 2638-2684.

https://doi.org/10.1002/(SICI)1521 3773(19990917)38:18<2638::AID-ANIE2638>3.0.CO;2-4

[2] A.K. Cheetham, G. Ferey, T. Loiseau, Open-framework inorganic materials, Angew. Chem. Int. Ed. 38 (1999) 3268-3292.

https://doi.org/10.1002/(SICI)1521-3773(19991115)38:22<3268::AID-ANIE3268>3.0.CO;2-U

[3] G. Ferey, Microporous solids: From organically templated inorganic skeletons to hybrid frameworks ecumenism in chemistry, Chem. Mater. 13 (2001) 3084-3098. https://doi.org/10.1021/cm011070n

[4] Z. Chen, J. Lv. K. Yu, H. Zhang, C. Wang, C. Wang & B. Zhou, Self-assembly, bifunctional electrocatalytic behavior, and photocatalytic property of host-guest metal-oxide-based coordination polymers, J Coord Chem. 69 (2016) 39-47. https://doi.org/10.1080/00958972.2015.1117074

[5] M. O'keeffe, M. Eddaoudi, Li. Hailian, T. Reineke, O.M. Yaghi, Frameworks for extended solids: geometrical design principles, J. Solid. State Chem. 152 (2000) 3-20. https://doi.org/10.1006/jssc.2000.8723

[6] R. Finn, J. Zubieta, Solid state coordination chemistry of oxovanadium phosphates: hydrothermal syntheses and structures of the network and chain phosphate phases $[\{Cu(bpy)\}_2(VO)_3(PO_4)_2(HPO_4)_2].2H_2O$ and $[\{Cu(terpy)\}_2(VO_2)_3(PO_4)(HPO_4)_2]$, Chem. Commun. (2000) 1321-1322. https://doi.org/10.1039/A909743K

[7] S.S.Y. Chui, S.M.F. Lo, J.P.H. Charmant, A.G. Orpen, I.D. Williams, A chemically functionalizable nanoporous material $[Cu_3(TMA)_2(H_2O)_3]_n$, Science. 238 (1999) 1148-1150. https://doi.org/10.1126/science.283.5405.1148

[8] W. Huang, D. Wu, P. Zhou, W. Yan, D. Guo, C. Duan, Q. Meng, Luminescent and magnetic properties of lanthanide-thiophene-2, 5-dicarboxylate hybrid materials, Cryst. Growth. Des. 9 (2009) 1361-1369. doi.org/10.1021/cg800531y

[9] T.M. Reineke, M. Eddaoudi, M. O'keeffe, O.M. Yaghi, A microporous lanthanide-organic framework, Angew. Chem. Int. Ed. 38 (1999) 2590-2594.

https://doi.org/10.1002/(SICI)1521-3773(19990903)38:17<2590::AID-ANIE2590>3.0.CO;2-H

[10] M. Eddaoudi, D.B. Moler, H. Li, B. Chen, T.M. Reineke, M. O'Keeffe, and O.M. Yaghi, Modular chemistry: secondary building units as a basis for the design of highly porous and robust metal-organic carboxylate frameworks, Acc. Chem. Res. 34 (2001) 319-330. https://doi.org/10.1021/ar000034b

[11] F. Millange, C. Serre, J. Marrot, N. Gardant, F. Pellé, G. Férey, Synthesis, structure and properties of a three-dimensional porous rare-earth carboxylate MIL-83 (Eu): $Eu_2(O_2C\text{-}C_{10}H_{14}\text{-}CO_2)_3$, J. Mater. Chem. 14 (2004) 642-645. https://doi.org/10.1039/B314343K

[12] J.Y. Hu, J. Wen, X-G. Yang, M. Chen, C.-S. Li, A 3-D lanthanide-organic framework based on in situ formed benzene-1,2,3,4-tetracarboxylate ligand. Inorg. Chem. Commun. 33 (2013) 25-28. https://doi.org/10.1016/j.inoche.2013.03.035

[13] M. Edgar, R. Mitchell, A.M.Z. Slawin, P. Lightfoot, P. Wright, A. Solid State Transformations of Zinc 1,4-Benzenedicarboxylates Mediated by Hydrogen-Bond-Forming Molecules, Chem. Eur. J. 7 (2001) 5168-5175.

https://doi.org/10.1002/1521-3765(20011203)7:23<5168::AID-CHEM5168>3.0.CO;2-S

[14] C. Livage, C. Egger, G. Férey, Hybrid Open Networks (MIL 16): Synthesis, Crystal Structure, and Ferrimagnetism of $Co_4(OH)_2(H_2O)_2(C_4H_4O_4)_3.2H_2O$, a New Layered Cobalt (II) Carboxylate with 14-Membered Ring Channels, Chem. Mater. 11 (1999) 1546-1550. https://doi.org/10.1021/cm980781r

[15] R. Sieber, S. Decurtins, H. Stoeckli-Evans, C. Wilson, D. Yufit, J.A.K. Howard, S.C. Capelli, A. Hauser. A Thermal Spin Transition in $[Co(bpy)_3][LiCr(ox)_3]$ (ox = $C_2O_4^{2-}$; bpy = 2,2'-bipyridine, Chem. Eur. J. 6 (2000) 361-368.

https://doi.org/10.1002/(SICI)1521-3765(20000117)6:2<361::AID-CHEM361>3.0.CO;2-Y

[16] E. Coronado, J.R. Galán-Mascarós, C.J. Gómez-García, J. Ensling, P. Gütlich, Hybrid Molecular Magnets Obtained by Insertion of Decamethylmetallocenium Cations into Layered, Bimetallic Oxalate Complexes: $[Z^{III}Cp^*_2][M^{II}M^{III}(ox)_3]$($Z^{III}$= Co, Fe; M^{III}= Cr, Fe; M^{II}= Mn, Fe, Co, Cu, Zn; ox= oxalate; Cp*= pentamethylcyclopentadienyl), Eur. J. Chem. 6 (2000) 552-563.

https://doi.org/10.1002/(SICI)1521-3765(20000204)6:3<552::AID-CHEM552>3.0.CO;2-U

[17] O. Hisashi, Y. Yukihiro, O. Kazuya, O. and H. Kitagawa, Network-Selectivity, Magnetism, and Proton Conduction of 2-D and 3-D Metal-Organic Frameworks of the Constituents $\{P(CH_2OH)_4\}^+/M^{II}$(Mn^{II}, Fe^{II}, or Co^{II})/$[Cr^{III}(ox)_3]^{3-}$, Inorg. Chem. 59 (2019) 623-628. https://doi.org/10.1021/acs.inorgchem.9b02861

[18] R. Pellaux, H.W. Schmalle, S. Decurtins, P. Fischer, F. Fauth, B. Ouladdiaf, T. Hauss, Magnetic structure of two-and three-dimensional supramolecular compounds, Physica B: Cond, Matter. 234 (1997) 783-784. https://doi.org/10.1016/S0921-4526(96)01164-7

[19] S. Natarajan, R. Vaidhyanathan, C.N.R. Rao, S. Ayyappan, A.K. Cheetham, Layered tin (II) oxalates possessing large apertures, Chem. Mater. 11 (1999) 1633-1639. https://doi.org/10.1021/cm990124e

[20] R. Vaidhyanathan, S. Natarajan, A.K. Cheetham, C.N.R. Rao, New open-framework zinc oxalates synthesized in the presence of structure-directing organic amines, Chem. Mater. 11 (1999) 3636-3642. https://doi.org/10.1021/cm990434x

[21] R. Vaidhyanathan, S. Natarajan, C.N.R. Rao, Synthesis of a hierarchy of zinc oxalate structures from amine oxalates, J. Chem. Soc. Dalton Trans. (2001) 699-706. https://doi.org/10.1039/B008571P

[22] T.D. Keene, H.R. Ogilvie, M.B. Hursthouse, D.J. Price, One-Dimensional Magnetism in New, Layered Structures: Piperazine-Linked Copper and Nickel Oxalate Chains, Eur. J. Inorg. Chem. 2004 (2004) 1007-1013. https://doi.org/10.1002/ejic.200300592

[23] F.A. Mautner, R.L. Febee and S.S. Massoud, Structural characterization of some oxalato-bridged copper (II) and nickel (II) complexes, J. Mol. Struct. 921 (2009) 333-340. https://doi.org/10.1016/j.molstruc.2009.01.031

[24] T.D. Keene, M.B. Hursthouse, D.J. Price, Stabilization of discrete $[Cu(C_2O_4)_2(H_2O)_2]^{2-}$ dianions in the solid state by an extensive hydrogen bonded network, Z. Anorg. Allg. Chem. 630 (2004) 350-352. https://doi.org/10.1002/zaac.200300373

[25] M. Akouibaa, N. Hamdi, H.H. Oudghiri. S. Rakib, M. Lachkar, I. da Silva, B. El Bali, $[Ni(N_2H_5)_2(C_2O_4)_2]\cdot 2H_2O$: Formation, crystal structure, catalytic performance and sorbence activities, Physica B: Condensed Matter. 635 (2022) 413857. https://doi.org/10.1016/j.physb.2022.413857

[26] Agilent (2010). CrysAlis PRO. Agilent Technologies, Yarnton, England.

[27] (a) SIR97: A. Altomare, M.C. Burla, M. Camalli, G.L. Cascarano, C. Giacovazzo, A. Guagliardi, A.G.G. Moliterni, G. Polidori, R. Spagna, a new tool for crystal structure determination and refinement, J. Appl. Cryst. 32 (1999) 115-119. https://doi.org/10.1107/S0021889898007717

(b) SUPERFLIP, L. Palatinus, G. Chapuis, A computer program for the solution of crystal structures by charge flipping in arbitrary dimensions, J. Appl. Cryst. 40 (2007) 786-790.

https://doi.org/10.1107/S0021889807029238

[28] V. Petříček, M. Dušek, L. Palatinus, Crystallographic Computing System JANA2006: General features, Z. Kristallogr. 229 (2014) 345-352. https://doi.org/10.1515/zkri-2014-1737

[29] K. Brandenburg, H. Putz, Crystal Impact GbR. Postfach 1251, D 53002 Bonn, 2005 Germany.

[30] Z.A. Savel'eva, S.V. Larionov, G.V. Romanenko, N.V. Podberezskaya, L.A. Sheludyakova, Zh. Neorg. Khim. Russ. J. Inorg. Chem. 37 (1992) 1094-1102.

[31] M.E. Fleet, Distortion parameters for coordination polyhedral, Mineral. Mag. 40 (1976) 531-533.

[32] K. Robinson, G.V. Gibbs, P.H. Ribbe, Quadratic elongation: a quantitative measure of distortion in coordination polyhedral, Science. 172 (3983) (1971) 567-570. https://doi:10.1126/science.172.3983.567

[33] B. El Bali, A. Boukhari, F. Abraham, J. Aride, The crystal structure of $SrNi_2(PO_4)_2$, J. Solid. State Chem. 104 (1993) 453-459. https://doi.org/10.1006/jssc.1993.1180

[34] C.R. Groom, I.J. Bruno, M.P. Lightfoot, S.C. Ward, The Cambridge Structural Database (CSD), Acta Cryst. B72 (2016) 171-179. https://doi.org/10.1107/S2052520616003954

[35] G. Karotsis, C. Stoumpos, A. Collins, F. White, S. Parsons, A.M.Z. Slawin, G.S. Papaefstathiou, E.K. Brechin, Molecular and supramolecular Ni(II) wheels from α-benzoin oxime, Dalton Trans. (2009) 3388-3390. https://doi.org/10.1039/B902002K

[36] L.G. Wang, A tetrahedrally coordinated Ag_I and Ni_{II} complex with a two-dimensional framework containing one-dimensional helical chains, Acta. Cryst. C63 (2007) m479-m480. doi.org/10.1107/S0108270107044794

[37] S.B. Wang, R.F. Li, G.M. Yang, D.Z. Liao, Z.H. Jiang, S.P. Yan, Three trinuclear Cu–M–Cu (M = Co, Ni and Zn) complexes including macrocyclic oxamido bridge: Synthesis, structures and magnetic properties, Inorg. Chim. Acta. 358 (2005) 2595-2601. https://doi.org/10.1016/j.ica.2005.03.017

[38] Q.W. Li, catena-[tetrakis(μ-aqua)-tetrakis(μ -hydroxo)-tetrakis(5-carboxythiophene-2-c

arboxylato)-tetra-nickel tetrahydrate], Private Communication CCDC 1497947 (2016).

[39] H.Q. Liu, Diaquabis(malato-K_2O,O')nickel(II), Acta Crystallogr. Sect. E63 (2007) m2470.

[40] I.D. Brown, D. Altermatt, Bond-valence parameters obtained from a systematic analysis of the Inorganic Crystal Structure Database, Acta. Cryst. B41 (1985) 244-247.

[41] T. Steiner, The Hydrogen Bond in the Solid State. Angew. Chem. Int. Ed. 41 (2002) 48-76. https://doi.org/10.1002/1521-3773(20020104)41:1<48::AID-ANIE48>3.0.CO;2-U.

[42] M. Narsimhulu, G.A. Kumar, G. Bhargavi, B. Srinivas, K.A. Hussain, Synthesis, crystal structure, thermal, photoluminescent and magnetic properties of a new material: $Na_2[Ni(C_2O_4)_2(H_2O)_2].6H_2O$, J. Mol. Struct. 1178 (2019) 155-161. https://doi.org/10.1016/j.molstruc.2018.10.013

[43] M. Shakir, A. Abbasi, M. Azam, A.U. Khan, Synthesis, spectroscopic studies and crystal structure of the Schiff base ligand L derived from condensation of 2-thiophenecarboxaldehyde and 3,3-diaminobenzidine and its complexes with Co(II), Ni(II), Cu(II), Cd(II) and Hg(II): Comparative DNA binding studies of L and its Co(II), Ni(II) and Cu(II) complexes, Spectrochim. Acta A Mol. Biomol. Spectrosc. 79 (2011) 1866-1875. https://doi.org/10.1016/j.saa.2011.05.077

[44] R. Stranger, K.L. McMahon, L.R. Gahan, J.I. Bruce, T.W. Hambley, Spin-Orbit Mixing and Nephelauxetic Effects in the Electronic Spectra of Nickel(II)-Encapsulating Complexes Involving Nitrogen and Sulfur Donors, Inorg. Chem. 36 (1997) 3466-3475. https://doi.org/10.1021/ic9614531

[45] F.A. Cotton, G. Wilkinson, Advanced Inorganic Chemistry, Fifth Edition; J. Wiley: New York, (1988) 745.

[46] G. Bussière, and C. Reber, Coupled Excited States in Nickel(II) Complexes Probed by Polarized Absorption Spectroscopy. J. Am. Chem. Soc. 120 (1998) 6306-6315. https://doi.org/10.1021/ja9740733

[47] M. Triest, G. Bussière, H. Bélisle, and C. Reber, Why Does the Middle Band in the Absorption Spectrum of $Ni(H_2O)_6^{2+}$ Have Two Maxima? J. Chem. Educ. 77 (2000) 670.

[48] A.H. Morrish, The physical principles of magnetism, IEEE New York (2001).

[49] C. Hess, Heat conduction in low-dimensional quantum magnets, Eur. Phys. J. Spec. Top. 151 (2007) 73-83. https://doi.org/10.1140/epjst/e2007-00363-8

[50] B.C. Melot, G Rousse, J.N. Chotard, M. Ati, J. Rodríguez-Carvajal, M.C. Kemei, J.M. Tarascon, Magnetic Structure and Properties of the Li-Ion Battery Materials $FeSO_4F$ and $LiFeSO_4F$, Chem. Mater. 23 (2011) 2922-2930. https://doi.org/10.1021/cm200465u

[51] B.C. Melot, J.-N. Chotard, G. Rousse, M. Ati, M. Reynaud,and J.M. Tarascon, Synthesis, structure and magnetic properties of the $NaCoXO_4F.2H_2O$ phases where X = S and Se, Inorg. Chem. 50 (2011) 7662-7668. https://doi.org/10.1021/ic200700r

[52] A.S. Borovik-romanov, V.R. Karasik, and N.M. Kreines, The Antiferromagnetism of Anhydrous Sulfates of Ni^{2+}, Fe^{2+}, Co^{2+} and Cu^{2+}, J. Exptl. Theoret. Phys. (1957) 4-18.

[53] A. Angermann, J. Töpfer, Synthesis of nanocrystalline Mn-Zn ferrite powders through thermolysis of mixed oxalates, Ceramics International. 37 (2011) 995-1002. https://doi.org/10.1016/j.ceramint.2010.11.019

[54] M.L. Feng, H.Y. Ye, J.G. Mao, Synthesis, crystal structures and photoluminescence properties of three novel organically bonded indium selenates or selenites, J. Solid. State Chem. 180 (2007) 2471-2477.

https://doi.org/10.1016/j.jssc.2007.06.022

[55] M. Trpkovska, B. Šoptrajanov, L. Pejov, Reinvestigation of the Infrared Spectra of Calcium Oxalate Monohydrate and its Partially Deuterated Analogues: An Experimental and Theoretical Study, Bull. Chem. Technol. Macedonia. 21 (2002) 110-116.

[56] K. Nagaraj, S. Ambika, S. Rajasri, S. Subramanian, A. Sankaralingam, Synthesis, micellization behavior, antimicrobial and intercalative DNA binding of some novel surfactant copper (II) complexes containing modified phenanthroline ligands. Colloids Surf. B. 122 (2014) 151-157. https://doi.org/10.1016/j.colsurfb.2014.05.011

[57] M. Al-Noaimi, M.I. Choudhary, F.F. Awwadi, W.H. Talib, T. Ben Hadda, S. Yousuf, A. Sawafta, I. Warad, Characterization and biological activities of two copper (II) complexes with dipropylenetriamine and diamine as ligands. Spectroc. Acta A. 127 (2014) 225-230.

https://doi.org/10.1016/j.saa.2014.02.016

[58] W. Yao, S.-H. Yu, J. Jiang, L. Zhang, Complex wurtzite ZnSe microspheres with high hierarchy and their optical properties, Chem. Eur. 12 (2006) 2066-2072. https://doi.org/10.1002/chem.200500835

[59] O. Rotthaus, F. Thomas, O. Jarjayes, C. Philouze, E. Saint-Aman, J-L. Pierre, Valence Tautomerism in Octahedral and Square-Planar Phenoxyl-Nickel (II) Complexes: Are Imino Nitrogen Atoms Good Friends? Eur. J. Chem. 12 (2006) 6953-6962. https://doi.org/10.1002/chem.200600258

[60] B.M. Gatehouse, S.E. Livingstone, R.S. Nyholm, Infrared spectra of some nitrato-co-ordination complexes, J. Chem. Soc. (Resumed) (1957) 4222-4225. https://doi.org/10.1039/JR9570004222

[61] P.H. Merrell, E.C. Alyea and L. Ecott, Synthesis and characterization of metal complexes of terdentate NNN donor ligands derived from 2, 6-diacetylpyridine. Nickel (II), copper (II), zinc (II) and cadmium (II) complexes of 2, 6-diacetylpyridinebis (anil) with both monodentate and bidentate nitrate groups, Inorg. Chim. Acta. 59 (1982) 25-32. https://doi.org/10.1016/S0020-1693(00)87303-X

[62] N.F. Curtis, Y.M. Curtis, Some nitrato-amine nickel (II) compounds with monodentate and bidentate nitrate ions, Inorg. Chem. 4 (1965) 804-809.

https://doi.org/10.1021/ic50028a007

[63] B.M. Gatehouse, A.E. Comyns, Infrared spectra of uranyl nitrate hydrates and rubidium uranyl nitrate, J. Chem. Soc. (Resumed) 802 (1958) 3965-3971.

https://doi.org/10.1039/JR9580003965

[64] K. Nakamoto, Infrared and Raman Spectra of Inorganic and Coordination Compounds, 5th Ed, Wiley: New York (1997).

[65] M. Tavassol, M. Montazerozohori, A. Masoudiasl, Z. Akbari, Th. Doert, E.M. Vazquez Lopez, S.J. Fatemi, Synthesis, spectral analysis, crystal structure, Hirshfeld surface analyses, thermal behavior of two new nickel complexes and usage as precursor for preparation of Ni/NiO nanoparticles, Polyhedron. 176 (2020) 114287. https://doi.org/10.1016/j.poly.2019.114287

[66] S. Vairam, T. Premkumar and S. Govindarajan, Trimellitate complexes of divalent transition metals with hydrazinium cation: Thermal and spectroscopic studies, J. Therm. Anal. Calorim. 100 (2010) 955-960. https://doi.org/10.1007/s10973-009-0459-8

[67] S. Hidaoui, N. Hamdi, M. Akouibaa, R. Benali-Cherif, E. Vaclav, M. Dusek, M. Lachkar, B. ElBali, Synthesis, crystal structure and catalytic activity of the new hybrid phosphate $(C_4H_{12}N_2)[Co(H_2O)_6](HPO_4)_2$, J Mol Struct. 1265 (2022) 133296. https://doi.org/10.1016/j.molstruc.2022.133296

[68] H.O. Hassani, F.T. Al Wadaani, Preparation, Characterization and Catalytic Activity of Nickel Molybdate ($NiMoO_4$) Nanoparticles, Molecules. 23 (2018) 273.

https://doi.org/10.3390/molecules23020273

[69] A. Goyal, S. Bansal, S. Singhal, Facile reduction of nitrophenols: Comparative catalytic efficiency of MFe_2O_4 (M = Ni, Cu, Zn) nano ferrites, Int. J. Hydrogen Energy. 39 (2014) 4895-4908. https://doi.org/10.1016/j.ijhydene.2014.01.050

[70] J. Xia, G. He, L. Zhang, X. Sun, X. Wang, Hydrogenation of nitrophenols catalyzed by carbon black-supported nickel nanoparticles under mild conditions, Appl. Catal. B-Environ. 180 (2016) 408-415. https://doi.org/10.1016/j.apcatb.2015.06.043

[71] H.O. Hassani, S. Rakass, M. Abboudi, A. Mohmoud, F. Al-Wadaani, Preparation and Characterization of α-Zinc Molybdate Catalyst: Efficient Sorbent for Methylene Blue and Reduction of 3-Nitrophenol, Molecules. 23 (2018) 1462. https://doi.org/10.3390/molecules23061462

[72] H.O Hassani, M. Akouibaa, S. Rakass, M. Abboudi, B. El Bali, M. Lachkar, F. Al Wadaani, A simple and cost-effective new synthesis method of copper molybdate $CuMoO_4$ nanoparticles and their catalytic performance, J. Sci.: Adv. Mater. Devices. 6 (2021) 501-507. https://doi.org/10.1016/j.jsamd.2021.06.003

[73] S. Pandey, S.B. Mishra, Catalytic reduction of p-nitrophenol by using platinum nanoparticles stabilised by guar gum, Carbohydr. Polym. 113 (2014) 525-531. https://doi.org/10.1016/j.carbpol.2014.07.047.

Supplementary file S1: CSD-Codes of the known crystal structures of Ni^{2+}-complexes with comparable Ni-O distances as in $(H_3dien)[Ni(NO_3)(C_2O_4)_2].2H_2O$.

ACACNI	AJEQOW	AQIYUV	AXUJUZ	AXUKAG	BECDIW	BIRMOH
BOWQAH	BUTHUU	CAKSOY	CIRMOI	CITWIM	COVWOA	COWTOY
DIHYUODOMXOT	DOMYAG	DUDCEN	DUVTUK	DUVWOH01	DUVWOH02	
EMILES	ENELIU	ETANAP	EXULEQ	FEDKIL	FOCREX	FOCRUN
FORSOX	FUXXIH	GAPKIS	GAWSIH	GEDDEA	GEHBUT	GOCFAG
GUJFEX	GUVQUK	HAGREO	HAJYEZ	HEGWOH	HIHPOF	HIPHIZ
HODLUK	HOLFIA	HORTOZ	HORTUF	HUHNED	HUHNIH	HUMXEU
HUMXIY	HUMXOE	HUMYOF	ICARUB	ICASAI	ICECAX	IDEROB
IGISOI	IVODOM	IXAZUC	JAKBEF	JEBWIZ	JEJMAP	JEYTOX
JOCPEZ	JUZKEW	KEKBAF	KIFPIB	KISBAQ	KISBEU	KOMCIA
LAKJIQ	LEJFAJ	LEKMUM	LIBMUG	LITGEB	LUXYAH	MALPUM
MIHMIZ	MIKXOW	MINNEF	MOLTEN	NAFYAU	NEJHAM	NIKMID
NIWQIV	NOHCIZ	NUTJAO	ONESOR	OPARUT	PAQJEY	PEDLOC
PEDMUJ	PELROP	PICLET	PITJEJ	PITJOT	PITKAG	POBXEK
POBXIO	POBXOU	POBYAH	POCDOD	PUQHAL	PUQHAL01	QIJSUZ
QODYAK	RAWZOG	REJQUT	REJQUT01	REJRAA	REJREE	REJRII
REJROO01	RIGRIJ	RUFKOT	SEZDOS	SICWEI	SICWIM	SICWOS
SICWUY	SICXAF	SUBWOD	SUBWOD01	SUJXUT	SULWIH	TEVHEJ
TIVSOH	TOQRUN	TUDNOW	TUDNUC	UFIPOO	UKEJAX	ULEHOK
ULUYAD	UZIKIY	UZILAR	VEHWIQ	VEHWOW	VINRUI	VINSAP
VOCCOH	WULJOF	XEYDAI	XEYDEM	XEZFIR	XEZFOX	XEZKUK
XEZMUM	XIDVOW	XIXMUP	XUDPOE	XUDQAR	XUDQEV	XUVYOF
YEVZEF	YOLYEF	YORPEC	YULKIA	YUSNUW	ZEKDAX	ZOKCIO